GEOLOGY

# The competing controls of glaciers, precipitation, and vegetation on high-mountain fluvial sediment yields

**Dongfeng Li[1,2,3,4]*, Ting Zhang[5]*, Desmond E. Walling[6], Stuart Lane[7], Bodo Bookhagen[8], Shang Tian[1,2], Irina Overeem[9], Jaia Syvitski[9], Albert J. Kettner[9], Edward Park[10], Michèle Koppes[11], Rafael J. P. Schmitt[12,13], Weiling Sun[1,2], Jinren Ni[1,2], Todd A. Ehlers[14]**



**Investigating erosion and river sediment yield in high-mountain areas is crucial for understanding landscape and biogeochemical responses to environmental change. We compile data on contemporary fluvial suspended sediment yield (SSY) and 12 environmental proxies from 151 rivers in High Mountain Asia surrounding the Tibetan Plateau. We demonstrate that glaciers exert a first-order control on fluvial SSYs, with high precipitation nonlinearly amplifying their role, especially in high–glacier cover basins. We find a bidirectional response to vegetation's influence on SSY in the Eastern Tibetan Plateau and Tien Shan and identify that the two interacting factors of precipitation and vegetation cover explain 54% of the variability in SSY, reflecting the divergent roles of vegetation in promoting biogenic-weathering versus slope stabilization across bioclimatic zones. The competing interactions between glaciers, ecosystems, and climate in delivering suspended sediment have important implications for predicting carbon and nutrient exports and water quality in response to future climate change.**

## INTRODUCTION

Climate change and glaciation drive rapid changes in erosion and sediment yield that are of major interest to the earth science community (*1*–*3*) and water-energy-environmental policy-makers (*4*–*6*). Glaciers carve mountain landscapes, limit mountain heights above the snowline [the "glacial buzzsaw"; (*7*)], and produce abundant readily mobilized sediment and associated bioavailable materials (e.g., carbon, nutrients, and contaminants) that further affect biodiversity, aquatic ecosystems, and downstream communities (*2*, *8*–*11*). At the catchment scale, basin-averaged erosion rates and sediment yields represent the net effect of glacial, fluvial, and mass-wasting processes that are further influenced by multiple competing factors including climate, vegetation, glaciation, tectonics, seismicity, lithology, and topography (*12*–*14*). However, our understanding of the relative importance and efficacy of these competing factors in regulating basin-averaged erosion and sediment yield across different timescales remains incomplete and the focus of ongoing debate (*13*, *15*–*17*). Here, we investigate and measure the competing influences of glaciers, vegetation, climate, and topography on contemporary fluvial sediment yield in the high-mountain areas of Asia.

High Mountain Asia (HMA) comprises the Tibetan Plateau and some of the planet's highest mountain ranges (e.g., Himalaya, Karakoram, Tienshan, Kunlun, Qilian, and Hengduan). HMA has been referred to as the Earth's third pole because it contains the planet's largest ice reservoir outside the Arctic and the Antarctic and serves as the headwaters of most large Asian rivers (*6*, *18*, *19*). These rivers transport water, sediment and dissolved material, nutrients, and organic carbon downstream, supporting four global biodiversity hot spots (i.e., the Himalaya hot spot, the Indo-Burma hot spot, the Mountains of Southwest China, and the Mountains of Central Asia) and the lives of approximately one-third of the world's population (*8*, *18*, *20*). Changes in fluvial water, sediment, and related nutrient and carbon fluxes have profound implications for downstream aquatic ecosystems, large human populations, and potential climate feedbacks (*2*, *10*, *21*). Existing HMA studies of erosion rates and sediment yields and their drivers mostly rely on millennial to million-year timescale basin-averaged erosion rates from cosmogenic radionuclides or low-temperature thermochronometry data (*15*, *22*, *23*). However, environmental factors influencing present-day fluvial sediment yields at the decadal-scale remain less studied across the entire HMA region.

Here, we present a compilation of present-day fluvial sediment yields and 12 environmental proxies from 151 quasi-pristine rivers located across HMA, including data from 47 previously unidentified catchments and 104 published values (1995–2015; see Materials and Methods). Our compilation represents a markedly expanded database compared to previous work (*24*–*27*) with the addition of environmental factors such as climate (precipitation and temperature), glacial cover, permafrost extent, lithology, topography, and vegetation cover. The influence of environmental factors on fluvial SSY was analyzed using multiple statistical approaches (correlation, partial least squares structural equation model, and random forest model) and the geographical detector (Geo-detector) *q*-statistic index (an index, ranging from 0 to 1, used to detect the extent to which an environmental variable and its interaction with other environmental variables can explain the spatial variability of the response variable; see Materials and Methods). We divide the HMA into five subregions for comparison to earlier studies (*5*, *28*) and the physiographic characteristics such as glacier and

[1]Key Laboratory for Water and Sediment Sciences, Ministry of Education, College of Environmental Sciences and Engineering, Peking University, Beijing 100871, China. [2]State Environmental Protection Key Laboratory of All Materials Flux in River Ecosystems, Peking University, Beijing 100871, China. [3]Institute of Carbon Neutrality, Peking University, Beijing 100871, China. [4]Institute of Tibetan Plateau, Peking University, Beijing 100871, China. [5]Center for Agricultural Water Research in China, College of Water Resources and Civil Engineering, China Agricultural University, Beijing 100083, China. [6]Department of Geography, Faculty of Environment, Science and Economy, University of Exeter, Exeter EX4 4RJ, UK. [7]Institute of Earth Surface Dynamics, University of Lausanne, Lausanne CH-1015, Switzerland. [8]Institute of Geosciences, Universität Potsdam, Potsdam 14476, Germany. [9]CSDMS, Institute of Arctic and Alpine Research, University of Colorado Boulder, Boulder, CO 80309, USA. [10]National Institute of Education, Earth Observatory of Singapore and Asian School of the Environment, Nanyang Technological University, Singapore. [11]Department of Geography, University of British Columbia, Vancouver, BC V6T1Z2, Canada. [12]Environmental Studies, University of California Santa Barbara, Santa Barbara, CA 93106, USA. [13]The Natural Capital Project and the Woods Institute for the Environment, Stanford University, Stanford, CA 94305, USA. [14]School of Geographical and Earth Sciences, University of Glasgow, G12 8QQ, Scotland, UK.
*Corresponding author. Email: dongfeng@u.nus.edu (D.L.); zhang_ting@u.nus.edu(T.Z.)

vegetation cover, climate, and topography. These regions include Qi Lian (QL), Eastern Tibetan Plateau (ETP), Himalaya–Karakoram–Hindu Kush (HKH), Kun Lun–Pamir (KLP), and Tien Shan (TS) (Fig. 1 and figs. S1 to S4). Our analysis focuses on mean annual suspended sediment yield (SSY; tons/km$^2$ per year), defined as the total amount of eroded sediment transported from a river basin in suspension per year, normalized by its drainage area (*29*, *30*).

## RESULTS

The mean annual SSYs in HMA are characterized by high spatial heterogeneity and vary between 21 (Jimai on the Yellow River, ETP) and 5481 (Shigar on the upper Indus River, HKH) tons/km$^2$ per year (Fig. 1A and table S1). The area-weighted SSYs for the mountain ranges are highest in HKH (987 ± 134 tons/km$^2$ per year, means ± SE), followed by TS (644 ± 99 tons/km$^2$ per year) and KLP (606 ± 103 tons/km$^2$ per year) and then QL (157 ± 43 tons/km$^2$ per year) and ETP (134 ± 13 tons/km$^2$ per year), respectively (Fig. 1A). The area-weighted mean glacier coverage is highest in HKH (10.28 ± 1.84%) and KLP (10.25 ± 1.02%), followed by TS (6.91 ± 1.35%), QL (1.49 ± 0.59%), and ETP (0.51 ± 0.12%), respectively. The mean annual normalized difference vegetation index (NDVI) is highest in ETP (0.32 ± 0.01), moderate in TS (0.17 ± 0.01) and QL (0.16 ± 0.02), and lowest in HKH (0.09 ± 0.01) and KLP (0.06 ± 0.01) (Fig. 1, A and B).

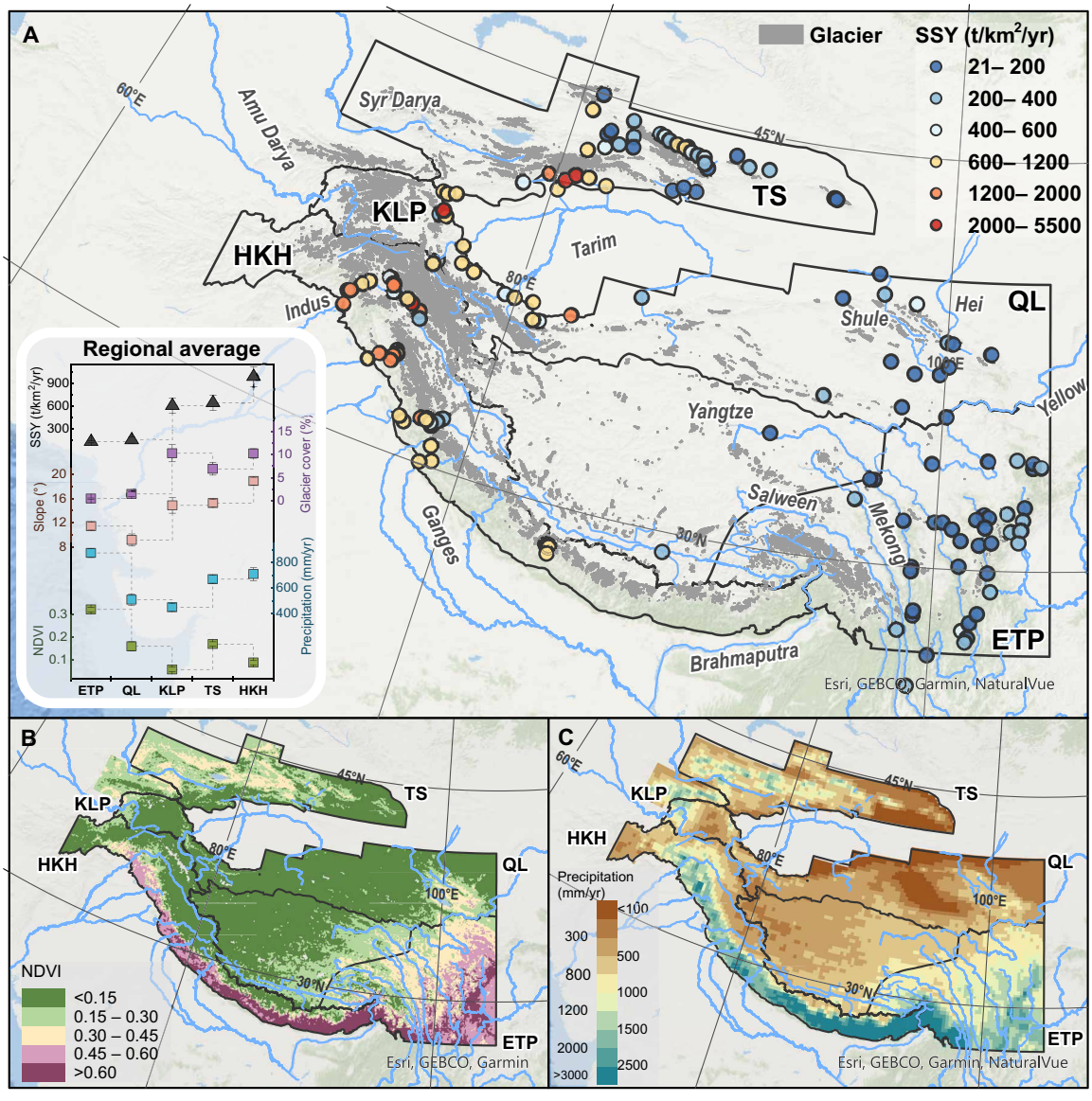


**Fig. 1. Spatial variations of SSY, vegetation cover, and precipitation in HMA.** (**A**) Spatial variation in contemporary mean annual SSY in the five subregions: Qi Lian (QL; 11 river basins), Eastern Tibetan Plateau (ETP; 44 river basins), Himalaya–Karakoram–Hindu Kush (HKH; 40 river basins), Kun Lun–Pamir (KLP; 16 river basins), and Tien Shan (TS; 40 river basins). The insert shows the area-weighted mean annual SSYs, glacier cover, mean annual normalized difference vegetation index (NDVI), and mean annual precipitation from the five subregions, with error bars denoting standard errors. The glacier map is based on the Randolph Glacier Inventory v7.0 (*28*). (**B**) Spatial variation in the mean annual NDVI. NDVI is based on the Global Inventory Modeling and Mapping Studies (GIMMS) NDVI product (*73*). (**C**) Spatial variation of mean annual precipitation. Precipitation is based on the ERA-5 reanalysis product (*74*). See tables S1 and S2 for details of the 151 selected quasi-undisturbed headwater river basins and the five subregions. mm/yr, millimeters per year; t/km$^2$/yr, tons per square kilometer per year.

The mean annual precipitation is highest in ETP (875 ± 35 mm) and HKH (710 ± 50 mm), moderate in TS (670 ± 30 mm) and QL (510 ± 45), and lowest in KLP (445 ± 30 mm) (Fig. 1, A and C). The basin-averaged slope (hillslope angle) is highest in HKH (18.86° ± 0.65°), followed by TS (15.24° ± 0.60°), KLP (14.85° ± 1.27°), ETP (11.46° ± 0.66°), and QL (9.17° ± 1°), respectively (Fig. 1A).

## DISCUSSION

### Influence of glaciers, precipitation, and topography

Statistical analysis indicates that glacier coverage is a crucial factor controlling SSY in HMA (Fig. 2). The selected quasi-pristine basins are classified into four categories: glacier-free basins (glacier cover < 0.1%; 30 basins), low–glacier cover basins (0.1% < glacier cover < 10%; 81 basins), moderate–glacier cover basins (10% < glacier cover < 20%; 33 basins), and high–glacier cover basins (glacier cover > 20%; 7 basins). Our analysis shows that the mean annual SSYs in high–glacier cover basins (2690 ± 540 tons/km$^2$ per year) are an order of magnitude greater than those in glacier-free basins (214 ± 33 tons/km$^2$ per year) (Fig. 2A). The SSYs demonstrate a strong positive correlation with glacier cover in HMA (coefficient of determination $r^2 = 0.62$, $P < 0.01$; Fig. 2B). The SSYs also display positive correlations with slope (Fig. 2B) and other topographical factors including relief and river channel steepness (factors reflecting tectonics, seismicity, and sediment connectivity and delivery) (fig. S5A).

The previous results support that the extent of basin-wide glacier cover represents an important driver of contemporary SSY, using only glacier cover or a few environmental factors (*24*, *31*). Basin-wide glacier cover can, to some extent, reflect ice volume or ice flux given the well-established scaling relation between glacier area and volume/thickness, as well as glacial activity (*1*, *3*, *13*). Glaciers are effective erosive agents, and, therefore sediment sources, erode and mobilize substantial amounts of sediment, especially in temperate and tectonically active mountain regions like HMA. This mobilized sediment is then exported downstream through subglacial drainage networks and proglacial streams (fig. S1, A and B) (*1*, *3*, *26*, *32*). The impact of glaciers on fluvial sediment yields may also reflect the role of paraglacial processes and sediment remobilization deposited during previous glacial advances (*33*), including from the Last Glacial Maximum (*34*, *35*) or the Little Ice Age (*36*). These factors lead to increased fluvial sediment yields through enhanced failures of debuttressed slopes (e.g., rockfalls and landslides), remobilization of glaciation-related sediment via fluvial processes (*37*, *38*), and the progressive development of increased connectivity between hillslopes and valley-bottom streams (fig. S1, C and D) (*39*). Restricted by the monitoring strategy for river sediment data (i.e., river gauging stations tend to be located at relatively distal locations from the glacier terminus), all our studied sites have a glacier cover extent of less than 50% (Fig. 2B), indirectly suggesting the potentially important role of paraglacial sedimentation, mass wasting, and fluvial readjustments in the glacier-free landscapes.

Comparison of SSY to environmental factors highlights their sensitivity to different factors. For example, we find that precipitation can amplify the roles of glaciers in regulating fluvial SSYs, especially in high–glacier cover basins (Fig. 3). In addition, the Geo-detector *q* statistic (an index, ranging from 0 to 1, used to detect the extent to which two interacting environmental variables can explain the spatial variability of the response variable; see Materials and Methods) for the two interacting factors of glacier cover, and mean annual precipitation is 0.72 and much higher than the *q* statistics for mean annual precipitation (0.01) and glacier cover (0.51) treated as single factors (fig. S5C). This suggests that the interaction between glacier cover and mean annual precipitation can explain 72% of the spatial variability of SSY in HMA. High mean annual precipitation can likely enhance glacial erosion through multiple mechanisms: more rainfall reaching the glacier bed, promoting sliding and expanding subglacial networks; and increased winter snowfall in the accumulation zone, promoting thicker ice, steeper mass balance gradients, and thus glacial erosion (*3*, *13*, *40*). High-magnitude rainstorms can also trigger other erosion events such as landslides, debris flows, and channel erosion in the downstream basin (*41*, *42*). In HKH, the high summer monsoonal rainfall coincides well with the widely

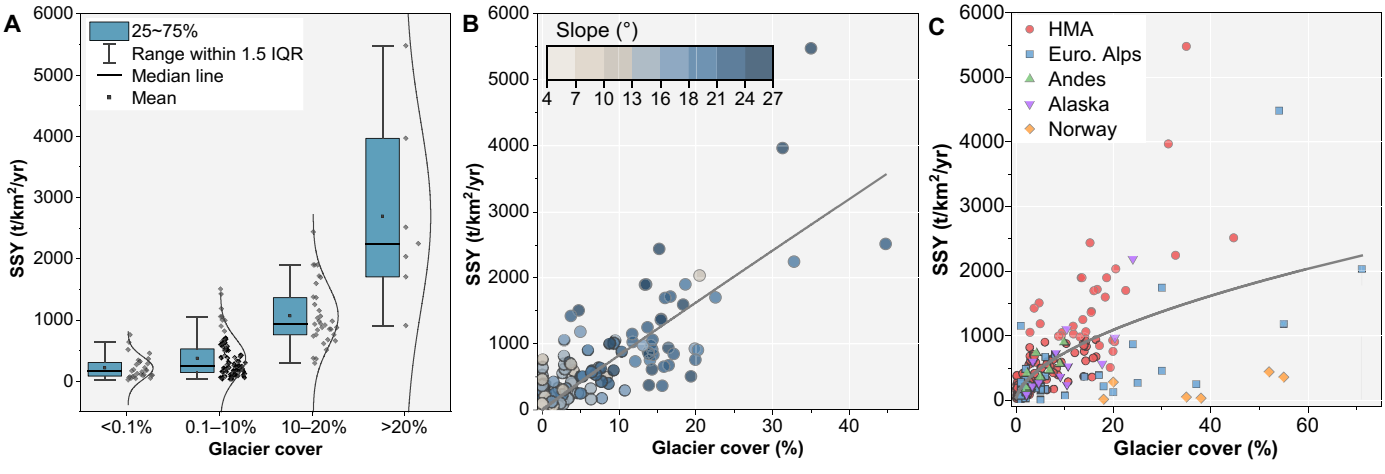


**Fig. 2. SSY as a function of percentage glacier cover.** (**A**) Variations in mean annual SSYs for glacier-free basins (glacier cover < 0.1%; 30 basins), low–glacier cover basins (0.1% < glacier cover < 10%; 81 basins), moderate–glacier cover basins (10% < glacier cover < 20%; 33 basins), and high–glacier cover basins (glacier cover > 20%; 7 basins). IQR, interquartile range. (**B**) Mean annual SSY as a function of percentage glacier cover in HMA ($y = 87.5x^{0.98}$, $r^2 = 0.62$, $P < 0.01$). (**C**) The dependence of mean annual SSY on percentage glacier cover in the world's cold regions. The correlation includes data from all the five cold regions ($y = 190x^{0.43}$, $r^2 = 0.34$, $P < 0.01$). See table S3 for the detailed SSYs in other cold regions. The gray-shaded areas denote the 95% confidence intervals.

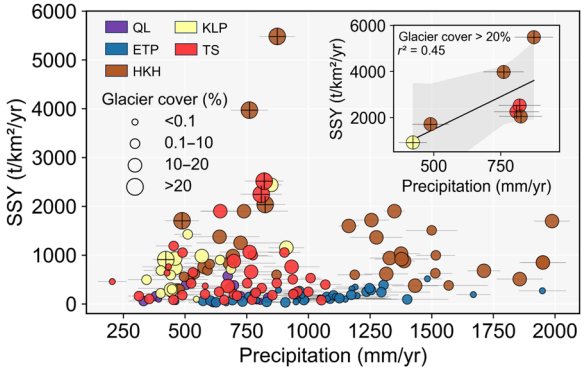


**Fig. 3. The observed relationship between SSY and mean annual precipitation conditioned by glacier cover (circle sizes).** The inset indicates that, in high–glacier cover basins (glacier cover > 20%; symbols marked with +), the SSYs increase with mean annual precipitation. Subregion labels correspond to those identified in Figs. 1 and 2. Error bars denote SD.

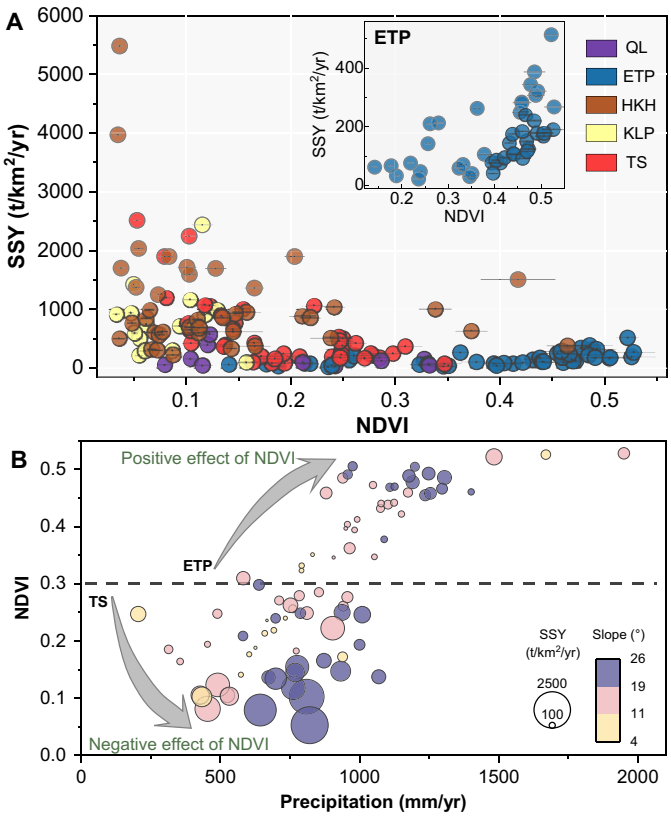


**Fig. 4. The observed relationship between SSY and vegetation cover (NDVI) and precipitation.** (**A**) SSY vegetation exhibits a bidirectional U-shaped pattern, with a negative exponential correlation with vegetation in TS ($y = 1633.6e^{-7.62x}$, $r^2 = 0.54$, $P < 0.01$) and a positive exponential correlation with vegetation in ETP (see the inset; $y = 20.32e^{4.60x}$, $r^2 = 0.39$, $P < 0.01$). An overall negative exponential correlation between SSYs and vegetation cover is indicated by the data from all the 151 basins ($y = 793.36e^{-3.78x}$, $r^2 = 0.26$, $P < 0.01$). Subregion labels correspond to those identified in Figs. 1 and 2. Error bars denote SD. (**B**) The observed relationship between SSY, NDVI, and mean annual precipitation conditioned by slope (circle sizes) in ETP and TS. A threshold of 0.3 is identified for the positive relationship between SSY and NDVI in ETP (larger SSY corresponds with larger NDVI) and the negative relationship between SSY and NDVI in TS (larger SSY corresponds with smaller NDVI).

documented rainfall-driven landslides (fig. S3), confirming the role of rainstorms in amplifying erosion and SSY. Furthermore, large volumes of sediment produced by glacial erosion and paraglacial erosion could be temporarily deposited in proglacial systems, awaiting high-magnitude precipitation events in combination with meltwater to remobilize the sediment and transport it further downstream (*43*–*45*). Such underlying mechanisms at least partly explain why the sediment yield in the relatively wet HKH (area-weighted SSY of ~1000 tons/km$^2$ per year, glacier cover of ~10%, mean annual precipitation of ~710 mm/year, and slope of ~19°) is much higher than that associated with the relatively dry KLP (area weighted SSY of ~600 tons/km$^2$ per year, glacier cover of ~10%, mean annual precipitation of ~450 mm/year, and slope of ~15°) (Fig. 1).

Furthermore, comparison of our results to other global mountain regions provides additional insights in SSY from glacierized regions. More specifically, our compilation of data shows that the mean annual SSYs in HMA's glacierized basins are close to those reported in Alaska with equivalent glacier cover but higher than those reported in the European Alps, Andes, and Norway with equivalent glacier cover (Fig. 2C). This is likely due to the steeper topography and higher monsoonal fluvial energy in HMA as compared to other glacierized mountain areas (*12*, *35*). Steep topography (relief and river channel steepness) has been linked to high tectonic uplift rates and seismic activities that can result in frequent landslides, high sediment connectivity, and thus high sediment yield (*15*, *23*). Tectonics and seismic activity in the European Alps, Andes, and Norway are overall less active than in HMA and Alaska, and the very resistant crystalline bedrock in Norway is another reason for its relatively low sediment yield (*24*, *31*, *43*, *46*). In addition, the high-magnitude summer monsoonal rainfall and stream power in the HKH region are powerful agents for fluvial incision, landslide (fig. S3) (*38*), and outburst floods (*4*, *42*), probably also contributing to the higher sediment yields.

## Divergent control of vegetation on sediment yield

We find a bidirectional U-shaped relationship between SSY and the vegetation index (NDVI) can be detected in ETP, TS, and HKH, although, in general, the SSYs display a significant negative relationship with the vegetation index for the whole dataset (Fig. 4). Specifically, the SSYs exhibit a significant positive exponential relationship with the vegetation index in the relative humid and heavily vegetated basins in ETP (mean annual precipitation of ~900 mm/year and NDVI of ~0.3 to 0.5) and a significant negative exponential relationship with the vegetation index in the relatively dry and sparsely vegetated basins in TS (mean annual precipitation of ~670 mm/year and NDVI of ~0.1 to 0.3). In HKH, the relationship between SSY and vegetation is characterized by a bidirectional U-shaped relationship, with a negative relationship (NDVI < 0.3) and a positive relationship (NDVI > 0.3). In contrast, no obvious positive or negative relationships are detected between SSY and the vegetation index in the other subregions of QL and KLP.

The positive relationship between SSY and vegetation cover in ETP reflects the interacting influences of vegetation, precipitation, and slope. The high annual precipitation found in southeastern ETP (1000 to 2000 mm/year; Figs. 1C and 4B) is influenced by the Indian monsoon and is associated with more frequent intense rainstorms

(*47*, *48*) that could increase erosion and thus sediment yield (fig. S3). The partial least squares structural equation model indicates that the role of vegetation in controlling SSY in ETP is largely derived from precipitation (fig. S6). We also find that, in ETP, the basins with denser vegetation cover are generally associated with steeper slopes that favor erosion (slopes over 20° for the basins with NDVI between 0.45 and 0.5; fig. S7). Furthermore, high annual precipitation is required to sustain dense vegetation cover (toward the southeastern part of ETP; Fig. 1, B and C) that likely has a stronger impact on enhancing weathering and erosion than on stabilizing the slopes and reducing erosion. Similar findings have also been reported from other high mountain areas such as the Andes (*14*) and East Africa (*49*). For instance, Starke and colleagues documented a strong positive correlation between $^{10}$Be-derived erosion rates and vegetation cover in the more densely vegetated and wetter region of the Andes (between 10°S and 14°S) (*14*). Such diverse erosion-vegetation cover relationships are also supported by the process-based landscape evolution model in high mountain areas (*50*).

The two interacting factors of mean annual precipitation and vegetation cover can explain 54% ($q$ statistic at 0.54) of the variability in SSY within HMA, which is much higher than that explained by either mean annual precipitation ($q$ statistic at 0.01) or vegetation ($q$ statistic at 0.25) alone (fig. S5C). This suggests that, in relatively humid regions (e.g., ETP), high mean annual precipitation enhances vegetation growth and is likely to boost biotic weathering (*14*), in addition to promoting surface runoff and associated erosion. In contrast, in relatively dry regions (e.g., TS), increased mean annual precipitation promotes vegetation growth, thereby inhibiting erosion and reducing sediment yield, while biotic weathering remains relatively low because of the limited vegetation cover density (NDVI < 0.3; Fig. 4A). Furthermore, our data show that the effects of temperature and lithology on SSY are overshadowed by the effects of differences in glacier cover (text S1 and figs. S8 and S9). For instance, the moderate-to-high–glacier cover basins are characterized by high sediment yields, but low mean annual temperatures and hard lithology and negative correlations are found between SSY and temperature/lithology.

## Implications and summary

Our study demonstrates the interacting roles of glaciers, vegetation, precipitation, and slope in mobilizing sediment and controlling contemporary fluvial SSYs. We highlight that the SSYs in high–glacier cover basins are on average an order of magnitude higher than glacier-free basins, and SSYs in Asia's glacierized catchments appear overall higher than those reported for the European Alps, the Andes, and Norway with equivalent glacier cover extents. The exceptionally high erosion and fluvial sediment yields from Asia's heavily glacierized mountain areas suggest the potential for more physical and biogeochemical threats to downstream water quality (e.g., large exports of fine-sediment–associated nutrients and contaminants), aquatic ecosystems (e.g., influences on biofilms, macroinvertebrates, and fish), river infrastructure (e.g., hydropower systems, bridges, and water intakes), and human environments (e.g., agriculture, pastoralism, heritage landscapes, and socioeconomic activities). For instance, more mercury and microplastic exports from glacier meltwater and glacier-derived fine sediment pose severe threats to water quality and river ecosystems on the Tibetan Plateau and downstream (*51*, *52*). High-magnitude erosion and river sediment transport events in glacierized basins in the Himalaya and other alpine settings could destroy river infrastructure including large hydropower systems and cultural heritage sites (*4*, *53*), as well as degrade aquatic biofilms and thus benthic macroinvertebrate and fish habitats (fig. S1, E and F) (*54*, *55*). In addition, glacial erosion and the large areas of fresh reactive mineral surfaces created or accelerated by glacier recession can likely enhance chemical weathering and carbon cycling (*2*, *11*, *56*), as evidenced by the much higher chemical weathering rates found in heavily glacierized basins than in glacier-free basins (*24*). However, the precise role of glacial erosion in enhancing chemical weathering and carbon cycling as well as the related timescales remains uncertain and an outstanding question to explore in the future.

Our results also indicate that precipitation can amplify the role of glaciers in controlling fluvial sediment yields (Fig. 3), possibly highlighting the role of precipitation in combining with ice melt to enhance basal sliding, glacial erosion, subglacial drainage networks, and sediment transport capacity. Given that global warming is frequently associated with more frequent extreme rainfall (*18*, *57*), the interacting roles of glaciers and precipitation suggest that, in the next decades, more intense warming-driven rainstorms will interact with deglaciation to influence mountain erosion and fluvial sediment yields. In the glacial basins of the Himalaya and Andes, there is emerging evidence of the interacting roles of precipitation and deglaciation in enhancing multi-decadal fine-sediment exports (*21*).

Our data provide evidence of a bidirectional U-shaped relationship between fluvial sediment yield and vegetation cover (Fig. 4A), reflecting the interacting influences of vegetation, precipitation, and slope angles. This finding corroborates the view that there are diverse erosion-vegetation relationships operating in different climatic zones worldwide (*14*, *58*), especially in mountain belts where climate, vegetation cover, and slope angles could vary substantially over a relatively small distance (*14*, *41*). The bidirectional relationship between sediment yield and vegetation also implies that, in the present-day dry zone (e.g., TS), the future erosion-vegetation relationship could possibly shift from a negative relationship toward a positive relationship, under future warming-wetting-greening scenarios (*18*, *19*). Such global change–driven dynamic erosion-vegetation relationships have profound implications for land management in high-mountain areas.

Together, the findings reported here suggest that, in the next few decades to centuries, mountain erosion and fluvial sediment yields will be jointly regulated by deglaciation, vegetation change, precipitation, as well as their interactions with slopes. Despite the positive relationship between fluvial sediment yield and glacier cover, we caution that glacier retreat and changes in glacier dynamics (*18*, *59*–*61*) in response to the 21st century global warming are unlikely to cause an immediate decrease in erosion and sediment yield. Instead, the unprecedented climate change and glacier retreat will likely enhance paraglacial erosion, expand thermally controlled erodible landscape, and thus increase fluvial sediment yield (*16*, *21*, *37*). Multi-decadal observations worldwide have demonstrated ice degradation-driven increases in sediment yields since the 1950s (*21*, *62*). The impact of warming-driven vegetation greening on slope stabilization and erosion reduction is likely to be complicated by the diversity of erosion-vegetation relationships and their conditioning by precipitation. Furthermore, global warming is frequently associated with more frequent extreme precipitation (*18*, *57*) that may interact with deglaciation and vegetation change to influence future fluvial sediment yields.

In conclusion, this study provides regionally extensive constraints on how multiple environmental factors influence present-day mountain

erosion and fluvial sediment yields in glacierized catchments. We highlight the importance of Asia's glacierized mountain rivers in providing not only strategically important water resources (*6*, *63*) but also the large potential for delivering high sediment loads and fine-sediment–associated carbon, nutrients, and contaminants (*2*, *51*). Our work elucidates the multiple competing factors in controlling basin-scale fluvial sediment yields and implies that the more accurate prediction of future fluvial sediment yields should rely on the explicit consideration of not only climate change (*18*) but also glacier dynamics and vegetation change as well as their interactions with slope. Such findings have important socio-ecological policy implications and suggest the necessity of using a systematic whole-basin approach for climate change adaptation in high-mountain areas, given the fundamental impacts of changing mountain erosion and fluvial sediment yields on agriculture, water quality, flood management, as well as the development of hydropower and other river-related infrastructure.

## MATERIALS AND METHODS

### Geographical setting

HMA encompasses the Tibetan Plateau and its surrounding Asian high mountains, such as the Himalaya, Karakoram, Hindu Kush, Kun Lun, TS, QL, and Hengduan (*5*, *18*). HMA also contains the Earth's largest ice reservoir outside the two polar regions and four global biodiversity hot spots in its diverse morphoclimatic zones (*8*, *20*). Recent studies have highlighted the importance of the HMA in terms of amplified climate change due to the elevation-dependent warming, rapid cryosphere degradation, and associated hydrogeomorphic and widespread societal impacts (*4*, *42*, *53*, *64*, *65*).

To examine the influence of different environmental factors on fluvial sediment yield in different morphoclimatic zones, the 151 selected river basins are grouped into five mountain ranges: QL (upper Hei-Shule River), ETP (upper Yellow-Yangtze-Mekong-Salween River), HKH (upper Brahmaputra-Ganges-Indus River), KLP (upper Tarim South River), and TS (upper Tarim North River). We divided the HMA into these five subregions by referring to the mountain range divisions of the subregions in the Randolph Glacier Inventory for HMA (*28*) and the Extended Hindu Kush Himalaya Region (*5*) and also considering their physiographic characteristics such as glaciers, vegetation and climate, as well as topography (Fig. 1). Specifically, QL represents a low-precipitation, low-glacier, moderate-vegetation region; ETP represents a high-precipitation, low-glacier, high-vegetation region; HKH represents a high-precipitation, high-glacier, low-vegetation region; KLP represents a low-precipitation, high-glacier, low-vegetation region; TS represents a moderate-precipitation, high-glacier, moderate-vegetation region.

### Selection of quasi-pristine glacierized and glacier-free river basins

As a basis for our analysis, we selected 151 quasi-pristine and largely unregulated headwater river basins located across HMA. Of these, 121 river basins are glacierized basins (glacier cover > 0.1%), and 30 basins are glacier-free basins (glacier cover < 0.1%), based on the latest Randolph Glacier Inventory v6.0 (*28*). Within these selected basins, the population density is low, and no large dams have affected the basin over the period of analysis (table S4). The very limited areas of agricultural land (<4%; fig. S2) are mostly located downstream of the hydrological monitoring stations at the basin outlets and restricted to the floodplains rather than the slopes of the catchments. This made it possible to preclude the potential impacts of various human activities on the fluvial sediment yields [e.g., water abstraction for agriculture and trapping of sediment in large reservoirs or changes in land use; (*27*, *30*, *66*)]. For the headwater basins where large dams were constructed during the investigation period (table S4), but the population was low and agricultural activity limited (fig. S2), we reconstructed the sediment yields for the post-dam period using the sediment yield/runoff relationships for the "pre-dam" periods.

### Data on fluvial SSY and basin-averaged environmental factors

#### *Data on SSY*

We collated and analyzed available contemporary fluvial SSY data from 151 quasi-pristine basins located across the entire HMA (47 previously unidentified compilations plus 104 published values; table S1) and also the associated environmental data (glacier cover, slope, vegetation, precipitation, drainage area, relief, temperature, lithology, runoff, and permafrost cover). The majority of the 151 selected river basins had records of sediment yield extending over at least 5 years, and 125 of them had records extending over at least 10 years (table S4); this selection criterion is critical to reduce the potential uncertainties caused by the interannual variations of sediment yield (*26*, *29*). For the river basins with multi-decadal observations of sediment yield, we selected the sediment yields covering the period 1995–2015 to match the environmental data for the same period. For instance, the glacier boundaries provided by the Randolph Glacier Inventory v7.0 are mostly derived from observations made during the period 1995–2015; we also used the vegetation and climate data covering the period 1995–2015.

The river runoff and SSY data for the 151 headwater basins are mostly based on hydrological stations within the framework of national monitoring programs managed by the Ministry of Water Resources, China; the Water and Power Development Authority, Pakistan; the Department of Hydrology and Meteorology, Nepal; and the Central Water Commission, India. Fluvial suspended sediment loads are measured throughout the melt season and the measured annual sediment load accounts for >90% of the total annual suspended sediment load. The measured annual suspended sediment loads (tons/year) are here reported as SSYs (tons/km$^2$ per year) to facilitate comparison between individual basins. For the Chinese monitoring stations (112 stations), suspended sediment is sampled once per day to determine the daily suspended sediment concentration (SSC) during low-flow periods when the SSC shows limited sub-daily variation. More frequent sub-daily samples are collected for periods during the flood season characterized by notable sub-daily variation of SSC. Both point and depth-integrated sampling coupled with cross-sectional measurements are undertaken. SSC values are determined by the conventional gravimetric/filtration approach (there are no reported changes in the SSC measurement procedure over the investigation period). The uncertainty associated with the sediment load data for the Chinese monitoring stations is reported to be less than 10%, according to the Chinese Hydrological Data Yearbook. SSY data for the rivers in India, Nepal, and Pakistan have been widely used in the literature (*17*, *25*, *67*), but detailed information on standardized sampling procedures and potential data uncertainty is not readily available.

We also carefully checked the original literature and removed those stations with measurement biases or where the loads reported were strongly influenced by human activities. For example, the SSY

data from the Ghousal and Tandi stations on the Indus River are not included in our analysis, because the data were deemed unreliable due to major underestimation when compared with downstream stations (*68*). Similarly, the sediment yield data from the station of Nar Khola in the Nepal Himalaya were excluded from our analysis, because the measured cross section was located within an unstable alluvial reach (*69*). In addition, a few river basins with specific sediment yields exceeding 6000 tons/km$^2$ per year as reported in (*26*) were excluded because of lack of coordinates and detailed/reliable sources. In addition, we checked the original annual time series of the fluvial SSYs in the upper Indus (HKH subregion) from the "Sediment Appraisal of Pakistan Rivers" and updated contemporary fluvial SSYs from the 1990s to 2000s as compared to those in (*18*, *67*) (stations S56 to S69 in table S4). The resulting carefully collated dataset is seen as representing the most comprehensive empirical information available to date on contemporary sediment yields in HMA.

Bedload fluxes can be high in high mountain rivers (20 to 60% of the total sediment load) (*30*, *31*, *70*), but, as with most rivers worldwide, they are not measured systematically in HMA and are notoriously challenging to model (*71*). Variations in the relative magnitude of bedload component between different rivers and at different measuring stations along the same river can be substantial as they reflect the influence of lithology, glacier cover, the efficiency of subglacial and fluvial quarrying and abrasion rates, hydraulic slope and grain size, as well as discharge (*70*, *71*). In this study, we therefore limited attention to fluvial SSY only.

### *Environmental data*

Environmental data such as the glacier cover, vegetation cover, precipitation, temperature, topography, lithology, and permafrost were also collected for use in exploring the factors influencing SSYs. The basin glacier cover was calculated using the latest Randolph Glacier Inventory v6.0 (*28*) (a globally complete inventory of glacier outlines compiled by the Global Land Ice Measurements from Space initiative; www.glims.org/RGI/). The distribution dates in the Randolph Glacier Inventory v6.0 have been set as close as possible to the year 2000, thus mostly falling within the period 1995–2015 and being consistent with the dates of the contemporary SSY data used in this study. Permafrost cover over the period of 2000–2016 was based on the dataset of "New high-resolution estimates of the permafrost thermal state and hydrothermal conditions over the Northern Hemisphere" that is available at the National Tibetan Plateau Data Center (*72*) (https://data.tpdc.ac.cn/en/data/5093d9ff-a5fc-4f10-a53f-c01e7b781368/).

The basin-averaged vegetation cover was computed using the NDVI data over the period 1995–2015 that are derived from the Global Inventory Modeling and Mapping Studies (GIMMS) group (*73*). In addition, we also compared the GIMMS NDVI product with the MODIS NDVI and found a very significant correlation between the two NDVI products, confirming the robustness of the NDVI data for the statistical analysis in this study (fig. S10).

The basin-averaged mean annual air temperature and annual precipitation were computed using the ERA-5 reanalysis climate dataset (European Centre for Medium-Range Weather Forecasts Reanalysis v5, https://cds.climate.copernicus.eu/). To match the sediment yield and glacier cover data that mostly cover the period 1995–2015, we also extracted the NDVI and ERA-5 reanalysis climate data covering the same period of 1995–2015. The ERA-5 reanalysis climate data are widely used in the cryosphere-hydrology-geomorphology analysis in HMA because of its improved spatial resolution and reduced biases compared to the earlier ERA-Interim (*74*, *75*).

Tectonically related topographic proxies such as relief, slope (hillslope angle), and river channel steepness were calculated using the Shuttle Radar Topography Mission (SRTM) digital elevation model (DEM) dataset with a spatial resolution of 90 m (https://earthexplorer.usgs.gov). The relief is the difference between the maximum elevation within a specific basin and the elevation at the related sediment monitoring station. The basin-averaged slope influences sediment connectivity and was derived using the slope analysis tool in the ArcGIS software (https://pro.arcgis.com/en/pro-app/2.8/tool-reference/spatial-analyst/how-slope-works.htm). The basin-averaged peak ground acceleration (PGA) was calculated using the Global Seismic Hazard Map at http://gmo.gfz-potsdam.de/pub/introduction/introduction_frame.html. The basin-averaged normalized river channel steepness ($K_{sn}$) also influences sediment connectivity and was computed using the MATLAB-based Topo Toolbox (*76*) (https://topotoolbox.wordpress.com/2020/07/23/calculating-basin-averaged-ksn-values/).

The basin-averaged lithology erodibility was computed using the Glim dataset of global lithologic distributions (*77*, *78*). The erodibility index of different lithology classes can be found in (*77*) and is not repeated here. The distribution of lithology in HMA is shown in fig. S4.

### Geo-detector *q*-statistic index

The Geo-detector *q* statistic (*79*) was used to quantify the relative importance of glacier cover, vegetation cover, mean annual precipitation, mean annual temperature, topography, lithology, basin area, and their interactions in influencing SSY. The Geo-detector *q*-statistic index builds on the theory of spatial stratification heterogeneity and is widely used in geospatial analysis to detect the extent to which an environmental variable (*X*) can explain the spatial variability of the response variable (*Y*) (*79*).

More specifically, the *q*-statistic index has a value ranging from 0 to 1. A high *q*-statistic index suggests a strong influence of *X* on *Y*. When the *q* statistic approaches 1, it means that *Y* is fully determined by *X* (i.e., *X* explains 100% of the spatial variation of *Y*). In addition to measuring the effect of a single factor, the *q* statistic can also quantify the effect of the interaction between two factors on the spatial variation of *Y*. In this study, *Y* refers to the SSY, and *X* refers to the key controlling variables of glacier cover, vegetation cover, precipitation, and topographic slope (fig. S5C). To reflect the potential interactions between multiple environmental factors and the associated nonlinear effects, it is possible to test the effect of both a single environmental factor *X* and the interaction of two environmental factors on the spatial variation of SSY (*Y*). The results of using the *q*-statistic index are shown in fig. S5C. The Geo-detector software and more details about the spatial stratified heterogeneity analysis are freely available at www.geodetector.cn/.

### Area-weighted average SSYs and environmental variables

Using the SSY values from the 151 gauging stations, we applied the area-weighted average approach to estimate the area-weighted mean SSY of the gauged basins in each subregion. Within each subregion, the weight of each gauged basin can be calculated as the ratio of the area of this gauged basin (excluding the overlapping areas for nested basins) to the total area of the gauged basins. This approach is also used to estimate the area-weighted mean of other environmental variables for the five subregions (Fig. 1A). Such an approach ensures a more accurate estimate of the fluvial SSY and associated environmental

variables for the gauged area than a simple arithmetic average approach, by assigning an increased weight for larger basins covering a greater proportion of the gauged area.

## Supplementary Materials

**This PDF file includes:**

Supplementary Text S1
Figs. S1 to S10
Tables S1 to S5

## REFERENCES AND NOTES


1. M. Koppes, B. Hallet, E. Rignot, J. Mouginot, J. S. Wellner, K. Boldt, Observed latitudinal variations in erosion as a function of glacier dynamics. *Nature* **526**, 100–103 (2015).
2. R. G. Hilton, A. J. West, Mountains, erosion and the carbon cycle. *Nat. Rev. Earth Environ.* **1**, 284–299 (2020).
3. F. Herman, F. De Doncker, I. Delaney, G. Prasicek, M. Koppes, The impact of glaciers on mountain erosion. *Nat. Rev. Earth Environ.* **2**, 422–435 (2021).
4. D. Li, X. Lu, D. E. Walling, T. Zhang, J. F. Steiner, R. J. Wasson, S. Harrison, S. Nepal, Y. Nie, W. W. Immerzeel, D. H. Shugar, M. Koppes, S. Lane, Z. Zeng, X. Sun, A. Yegorov, T. Bolch, High Mountain Asia hydropower systems threatened by climate-driven landscape instability. *Nat. Geosci.* **15**, 520–530 (2022).
5. T. Bolch, J. M. Shea, S. Liu, F. M. Azam, Y. Gao, S. Gruber, W. W. Immerzeel, A. Kulkarni, H. Li, A. A. Tahir, G. Zhang, Y. Zhang, "Status and Change of the Cryosphere in the Extended Hindu Kush Himalaya Region" in *The Hindu Kush Himalaya Assessment: Mountains, Climate Change, Sustainability and People*, P. Wester, A. Mishra, A. Mukherji, A. B. Shrestha, Eds. (Springer International Publishing, 2019), pp. 209–255; https://doi.org/10.1007/978-3-319-92288-1_7.
6. W. W. Immerzeel, A. F. Lutz, M. Andrade, A. Bahl, H. Biemans, T. Bolch, S. Hyde, S. Brumby, B. J. Davies, A. C. Elmore, A. Emmer, M. Feng, A. Fernández, U. Haritashya, J. S. Kargel, M. Koppes, P. D. A. Kraaijenbrink, A. V. Kulkarni, P. A. Mayewski, S. Nepal, P. Pacheco, T. H. Painter, F. Pellicciotti, H. Rajaram, S. Rupper, A. Sinisalo, A. B. Shrestha, D. Viviroli, Y. Wada, C. Xiao, T. Yao, J. E. M. Baillie, Importance and vulnerability of the world's water towers. *Nature* **577**, 364–369 (2020).
7. D. L. Egholm, S. B. Nielsen, V. K. Pedersen, J. E. Lesemann, Glacial effects limiting mountain height. *Nature* **460**, 884–887 (2009).
8. A. Antonelli, W. D. Kissling, S. G. A. Flantua, M. A. Bermúdez, A. Mulch, A. N. Muellner-Riehl, H. Kreft, H. P. Linder, C. Badgley, J. Fjeldså, S. A. Fritz, C. Rahbek, F. Herman, H. Hooghiemstra, C. Hoorn, Geological and climatic influences on mountain biodiversity. *Nat. Geosci.* **11**, 718–725 (2018).
9. I. Overeem, B. D. Hudson, J. P. M. Syvitski, A. B. Mikkelsen, B. Hasholt, M. R. van den Broeke, B. P. Y. Noël, M. Morlighem, Substantial export of suspended sediment to the global oceans from glacial erosion in Greenland. *Nat. Geosci.* **10**, 859–863 (2017).
10. A. M. Milner, K. Khamis, T. J. Battin, J. E. Brittain, N. E. Barrand, L. Füreder, S. Cauvy-Fraunié, G. M. Gíslason, D. Jacobsen, D. M. Hannah, A. J. Hodson, E. Hood, V. Lencioni, J. S. Ólafsson, C. T. Robinson, M. Tranter, L. E. Brown, Glacier shrinkage driving global changes in downstream systems. *Proc. Natl. Acad. Sci. U.S.A.* **114**, 9770–9778 (2017).
11. T. S. Bianchi, L. M. Mayer, J. H. F. Amaral, S. Arndt, V. Galy, D. B. Kemp, S. A. Kuehl, N. J. Murray, P. Regnier, Anthropogenic impacts on mud and organic carbon cycling. *Nat. Geosci.* **17**, 287–297 (2024).
12. J. P. M. Syvitski, J. D. Milliman, Geology, geography, and humans battle for dominance over the delivery of fluvial sediment to the coastal ocean. *J. Geol.* **115**, 1–19 (2007).
13. S. J. Cook, D. A. Swift, M. P. Kirkbride, P. G. Knight, R. I. Waller, The empirical basis for modelling glacial erosion rates. *Nat. Commun.* **11**, 759 (2020).
14. J. Starke, T. A. Ehlers, M. Schaller, Latitudinal effect of vegetation on erosion rates identified along western South America. *Science* **367**, 1358–1361 (2020).
15. S. M. Olen, B. Bookhagen, M. R. Strecker, Role of climate and vegetation density in modulating denudation rates in the Himalaya. *Earth Planet. Sci. Lett.* **445**, 57–67 (2016).
16. M. N. Koppes, D. R. Montgomery, The relative efficacy of fluvial and glacial erosion over modern to orogenic timescales. *Nat. Geosci.* **2**, 644–647 (2009).
17. S. Bhattacharjee, B. Bookhagen, R. Sinha, Sediment-transport rates from decadal to millennial timescales across the Indo-Gangetic Plain: Impacts of tectonics, climatic processes, and vegetation cover. *Earth Sci. Rev.* **233**, 104165 (2022).
18. D. Li, X. Lu, I. Overeem, D. E. Walling, J. Syvitski, A. J. Kettner, B. Bookhagen, Y. Zhou, T. Zhang, Exceptional increases in fluvial sediment fluxes in a warmer and wetter High Mountain Asia. *Science* **374**, 599–603 (2021).
19. T. Yao, Y. Xue, D. Chen, F. Chen, L. Thompson, P. Cui, T. Koike, W. K.-M. Lau, D. Lettenmaier, V. Mosbrugger, R. Zhang, B. Xu, J. Dozier, T. Gillespie, Y. Gu, S. Kang, S. Piao, S. Sugimoto, K. Ueno, L. Wang, W. Wang, F. Zhang, Y. Sheng, W. Guo, Ailikun, X. Yang, Y. Ma, S. S. P. Shen, Z. Su, F. Chen, S. Liang, Y. Liu, V. P. Singh, K. Yang, D. Yang, X. Zhao, Y. Qian, Y. Zhang, Q. Li, Recent third pole's rapid warming accompanies cryospheric melt and water cycle intensification and interactions between monsoon and environment: Multidisciplinary approach with observations, modeling, and analysis. *Bull. Am. Meteorol. Soc.* **100**, 423–444 (2019).
20. T. Zhang, D. Li, A. E. East, D. E. Walling, S. Lane, I. Overeem, A. A. Beylich, M. Koppes, X. Lu, Warming-driven erosion and sediment transport in cold regions. *Nat. Rev. Earth Environ.* **3**, 832–851 (2022).
21. V. Godard, D. L. Bourlès, F. Spinabella, D. W. Burbank, B. Bookhagen, G. B. Fisher, A. Moulin, L. Léanni, Dominance of tectonics over climate in Himalayan denudation. *Geology* **42**, 243–246 (2014).
22. B. A. Adams, K. X. Whipple, A. M. Forte, A. M. Heimsath, K. V. Hodges, Climate controls on erosion in tectonically active landscapes. *Sci. Adv.* **6**, eaaz3166 (2020).
23. B. Hallet, L. Hunter, J. Bogen, Rates of erosion and sediment evacuation by glaciers: A review of field data and their implications. *Glob. Planet. Change* **12**, 213–235 (1996).
24. H. Wulf, B. Bookhagen, D. Scherler, Climatic and geologic controls on suspended sediment flux in the Sutlej River Valley, western Himalaya. *Hydrol. Earth Syst. Sci.* **16**, 2193–2217 (2012).
25. J. L. Carrivick, F. S. Tweed, Deglaciation controls on sediment yield: Towards capturing spatio-temporal variability. *Earth Sci. Rev.* **221**, 103809 (2021).
26. L. Li, J. Ni, F. Chang, Y. Yue, N. Frolova, D. Magritsky, A. G. L. Borthwick, P. Ciais, Y. Wang, C. Zheng, D. E. Walling, Global trends in water and sediment fluxes of the world's large rivers. *Sci. Bull.* **65**, 62–69 (2020).
27. W. T. Pfeffer, A. A. Arendt, A. Bliss, T. Bolch, J. G. Cogley, A. S. Gardner, J.-O. Hagen, R. Hock, G. Kaser, C. Kienholz, E. S. Miles, G. Moholdt, N. Mölg, F. Paul, V. Radić, P. Rastner, B. H. Raup, J. Rich, M. J. Sharp, The Randolph Consortium, The Randolph Glacier Inventory: A globally complete inventory of glaciers. *J. Glaciol.* **60**, 537–552 (2014).
28. D. E. Walling, The sediment delivery problem. *J. Hydrol.* **65**, 209–237 (1983).
29. C. J. Tucker, J. E. Pinzon, M. E. Brown, D. A. Slayback, E. W. Pak, R. Mahoney, E. F. Vermote, N. El Saleous, An extended AVHRR 8-km NDVI dataset compatible with MODIS and SPOT vegetation NDVI data. *Int. J. Remote Sens.* **26**, 4485–4498 (2005).
30. H. Hersbach, B. Bell, P. Berrisford, S. Hirahara, A. Horányi, J. Muñoz Sabater, J. Nicolas, C. Peubey, R. Radu, D. Schepers, A. Simmons, C. Soci, S. Abdalla, X. Abellan, G. Balsamo, P. Bechtold, G. Biavati, J. Bidlot, M. Bonavita, G. Chiara, P. Dahlgren, D. Dee, M. Diamantakis, R. Dragani, J. Flemming, R. Forbes, M. Fuentes, A. Geer, L. Haimberger, S. Healy, R. J. Hogan, E. Hólm, M. Janisková, S. Keeley, P. Laloyaux, P. Lopez, C. Lupu, G. Radnoti, P. Rosnay, I. Rozum, F. Vamborg, S. Villaume, J. N. Thépaut, The ERA5 global reanalysis. *Q. J. R. Meteorol. Soc.* **146**, 1999–2049 (2020).
31. M. Church, J. M. Ryder, Paraglacial sedimentation: A consideration of fluvial processes conditioned by glaciation. *Geol. Soc. Am. Bull.* **83**, 3059–3072 (1972).
32. Q. Yan, L. A. Owen, Z. Zhang, H. Wang, T. Wei, N. Jiang, R. Zhang, Divergent evolution of glaciation across high-mountain Asia during the last four glacial-interglacial cycles. *Geophys. Res. Lett.* **48**, e2021GL092411 (2021).
33. P. D. Clift, T. N. Jonell, Monsoon controls on sediment generation and transport: Mass budget and provenance constraints from the Indus River catchment, delta and submarine fan over tectonic and multimillennial timescales. *Earth Sci. Rev.* **220**, 103682 (2021).
34. E. Lee, J. L. Carrivick, D. J. Quincey, S. J. Cook, W. H. M. James, L. E. Brown, Accelerated mass loss of Himalayan glaciers since the Little Ice Age. *Sci. Rep.* **11**, 24284 (2021).
35. M. Church, O. Slaymaker, Disequilibrium of Holocene sediment yield in glaciated British Columbia. *Nature* **337**, 452–454 (1989).
36. M. Fort, Glaciers and mass wasting processes: Their influence on the shaping of the Kali Gandaki valley (higher Himalaya of Nepal). *Quat. Int.* **65-66**, 101–119 (2000).
37. S. N. Lane, M. Bakker, C. Gabbud, N. Micheletti, J.-N. Saugy, Sediment export, transient landscape response and catchment-scale connectivity following rapid climate warming and Alpine glacier recession. *Geomorphology* **277**, 210–227 (2017).
38. D. A. Swift, P. W. Nienow, T. B. Hoey, Basal sediment evacuation by subglacial meltwater: Suspended sediment transport from Haut Glacier d'Arolla, Switzerland. *Earth Surf. Process. Landf.* **30**, 867–883 (2005).
39. B. Bookhagen, R. C. Thiede, M. R. Strecker, Abnormal monsoon years and their control on erosion and sediment flux in the high, arid northwest Himalaya. *Earth Planet. Sci. Lett.* **231**, 131–146 (2005).
40. K. L. Cook, C. Andermann, F. Gimbert, B. R. Adhikari, N. Hovius, Glacial lake outburst floods as drivers of fluvial erosion in the Himalaya. *Science* **362**, 53–57 (2018).
41. A. A. Beylich, K. Laute, J. E. A. Storms, Contemporary suspended sediment dynamics within two partly glacierized mountain drainage basins in western Norway (Erdalen and Bødalen, inner Nordfjord). *Geomorphology* **287**, 126–143 (2017).
42. T. Heckmann, S. McColl, D. Morche, Retreating ice: Research in pro-glacial areas matters. *Earth Surf. Process. Landf.* **41**, 271–276 (2016).
43. F. Zhang, C. Zeng, G. Wang, L. Wang, X. Shi, Runoff and sediment yield in relation to precipitation, temperature and glaciers on the Tibetan Plateau. *Int. Soil Water Conserv. Res.* **10**, 197–207 (2021).

44. J. Bogen, Glacial sediment production and development of hydro-electric power in glacierized areas. *Ann. Glaciol.* **13**, 6–11 (1989).
45. B. Bookhagen, D. W. Burbank, Toward a complete Himalayan hydrological budget: Spatiotemporal distribution of snowmelt and rainfall and their impact on river discharge. *J. Geophys. Res.* **115**, F03019 (2010).
46. V. Torres Acosta, T. F. Schildgen, B. A. Clarke, D. Scherler, B. Bookhagen, H. Wittmann, F. von Blanckenburg, M. R. Strecker, Effect of vegetation cover on millennial-scale landscape denudation rates in East Africa. *Lithosphere* **7**, 408–420 (2015).
47. M. Schmid, T. A. Ehlers, C. Werner, T. Hickler, J.-P. Fuentes-Espoz, Effect of changing vegetation and precipitation on denudation–Part 2: Predicted landscape response to transient climate and vegetation cover over millennial to million-year timescales. *Earth Surf. Dyn.* **6**, 859–881 (2018).
48. S. Sun, S. Kang, Q. Zhang, J. Guo, X. Sun, Research progress on behaviors and environmental effects of mercury in the cryosphere of the Tibetan Plateau: A critical review. *Sci. Cold Arid Reg.* **14**, 1–22 (2022).
49. C. Jiang, L. Yin, Z. Li, X. Wen, X. Luo, S. Hu, H. Yang, Y. Long, B. Deng, L. Huang, Y. Liu, Microplastic pollution in the rivers of the Tibet Plateau. *Environ. Pollut.* **249**, 91–98 (2019).
50. D. H. Shugar, M. Jacquemart, D. Shean, S. Bhushan, K. Upadhyay, A. Sattar, W. Schwanghart, S. McBride, M. de Vries, M. Mergili, A. Emmer, C. Deschamps-Berger, M. McDonnell, R. Bhambri, S. Allen, E. Berthier, J. L. Carrivick, J. J. Clague, M. Dokukin, S. A. Dunning, H. Frey, S. Gascoin, U. K. Haritashya, C. Huggel, A. Kaab, J. S. Kargel, J. L. Kavanaugh, P. Lacroix, D. Petley, S. Rupper, M. F. Azam, S. J. Cook, A. P. Dimri, M. Eriksson, D. Farinotti, J. Fiddes, K. R. Gnyawali, S. Harrison, M. Jha, M. Koppes, A. Kumar, S. Leinss, U. Majeed, S. Mal, A. Muhuri, J. Noetzli, F. Paul, I. Rashid, K. Sain, J. Steiner, F. Ugalde, C. S. Watson, M. J. Westoby, A massive rock and ice avalanche caused the 2021 disaster at Chamoli, Indian Himalaya. *Science* **373**, 300–306 (2021).
51. M. Roncoroni, D. Mancini, F. Miesen, T. Müller, M. Gianini, B. Ouvry, M. Clémençon, F. Lardet, T. J. Battin, S. N. Lane, Decrypting the stream periphyton physical habitat of recently deglaciated floodplains. *Sci. Total Environ.* **867**, 161374 (2023).
52. X. Li, N. Wang, Y. Ding, J. R. Hawkings, J. C. Yde, R. Raiswell, J. Liu, S. Zhang, S. Kang, R. Wang, Q. Liu, S. Liu, R. Bol, X. You, G. Li, Globally elevated chemical weathering rates beneath glaciers. *Nat. Commun.* **13**, 407 (2022).
53. A. K. Mishra, C. Placzek, R. Jones, Coupled influence of precipitation and vegetation on millennial-scale erosion rates derived from $^{10}$Be. *PLOS ONE* **14**, e0211325 (2019).
54. F. Brun, E. Berthier, P. Wagnon, A. Kääb, D. Treichler, A spatially resolved estimate of High Mountain Asia glacier mass balances from 2000 to 2016. *Nat. Geosci.* **10**, 668–673 (2017).
55. A. Dehecq, N. Gourmelen, A. S. Gardner, F. Brun, D. Goldberg, P. W. Nienow, E. Berthier, C. Vincent, P. Wagnon, E. Trouvé, Twenty-first century glacier slowdown driven by mass loss in High Mountain Asia. *Nat. Geosci.* **12**, 22–27 (2019).
56. J. Li, G. Wang, C. Song, S. Sun, J. Ma, Y. Wang, L. Guo, D. Li, Recent intensified erosion and massive sediment deposition in Tibetan Plateau rivers. *Nat. Commun.* **15**, 722 (2024).
57. P. Wester, A. Mishra, A. Mukherji, A. B. Shrestha, *The Hindu Kush Himalaya Assessment* (Springer, 2019).
58. M. F. Azam, J. S. Kargel, J. M. Shea, S. Nepal, U. K. Haritashya, S. Srivastava, F. Maussion, N. Qazi, P. Chevallier, A. P. Dimri, A. V. Kulkarni, J. G. Cogley, I. M. Bahuguna, Glaciohydrology of the Himalaya-Karakoram. *Science* **373**, eabf3668 (2021).
59. Y. Nie, H. D. Pritchard, Q. Liu, T. Hennig, W. Wang, X. Wang, S. Liu, S. Nepal, D. Samyn, K. Hewitt, X. Chen, Glacial change and hydrological implications in the Himalaya and Karakoram. *Nat. Rev. Earth Environ.* **2**, 91–106 (2021).
60. K. F. Ali, D. H. D. Boer, Spatial patterns and variation of suspended sediment yield in the upper Indus River basin, northern Pakistan. *J. Hydrol.* **334**, 368–387 (2007).
61. S. V. N. Rao, M. V. Rao, K. S. Ramasastri, R. N. P. Singh, A study of sedimentation in Chenab basin in western Himalayas. *Hydrol. Res.* **28**, 201–216 (1997).
62. E. Gabet, D. Burbank, B. Pratt-Sitaula, J. Putkonen, B. Bookhagen, Modern erosion rates in the High Himalayas of Nepal. *Earth Planet. Sci. Lett.* **267**, 482–494 (2008).
63. J. Syvitski, J. R. Ángel, Y. Saito, I. Overeem, C. J. Vörösmarty, H. Wang, D. Olago, Earth's sediment cycle during the Anthropocene. *Nat. Rev. Earth Environ.* **3**, 179–196 (2022).
64. J. M. Turowski, D. Rickenmann, S. J. Dadson, The partitioning of the total sediment load of a river into suspended load and bedload: A review of empirical data. *Sedimentology* **57**, 1126–1146 (2010).
65. S. Cohen, J. Syvitski, T. Ashely, R. Lammers, B. Fekete, H.-Y. Li, Spatial trends and drivers of bedload and suspended sediment fluxes in global rivers. *Water Resour. Res.* **58**, e2021WR031583 (2022).
66. Y. Ran, X. Li, G. Cheng, J. Che, J. Aalto, O. Karjalainen, J. Hjort, M. Luoto, H. Jin, J. Obu, M. Hori, Q. Yu, X. Chang, New high-resolution estimates of the permafrost thermal state and hydrothermal conditions over the Northern Hemisphere. *Earth Syst Sci Data* **14**, 865–884 (2022).
67. W. Schwanghart, D. Scherler, Short Communication: TopoToolbox 2–MATLAB-based software for topographic analysis and modeling in Earth surface sciences. *Earth Surf. Dyn.* **2**, 1–7 (2014).
68. N. Moosdorf, S. Cohen, C. von Hagke, A global erodibility index to represent sediment production potential of different rock types. *Appl. Geogr.* **101**, 36–44 (2018).
69. J. Hartmann, N. Moosdorf, The new global lithological map database GLiM: A representation of rock properties at the Earth surface. *Geochem. Geophys. Geosystems* **13**, Q12004 (2012).
70. J.-F. Wang, T.-L. Zhang, B.-J. Fu, A measure of spatial stratified heterogeneity. *Ecol. Indic.* **67**, 250–256 (2016).
71. L. Mao, R. Carrillo, Temporal dynamics of suspended sediment transport in a glacierized Andean basin. *Geomorphology* **287**, 116–125 (2017).
72. J. R. Slosson, C. Kelleher, G. D. Hoke, Contrasting impacts of a hotter and drier future on streamflow and catchment scale sediment flux in the High Andes. *J. Geophys. Res. Earth Surf.* **126**, e2021JF006182 (2021).
73. M. Hinderer, M. Kastowski, A. Kamelger, C. Bartolini, F. Schlunegger, River loads and modern denudation of the Alps—A review. *Earth Sci. Rev.* **118**, 11–44 (2013).
74. G. Antoniazza, S. N. Lane, Sediment yield over glacial cycles: A conceptual model. *Prog. Phys. Geogr. Earth Environ.* **45**, 842–865 (2021).
75. G. L. Guymon, Regional sediment yield analysis of Alaska streams. *J. Hydraul. Div.* **100**, 41–51 (1974).
76. A. Elverhøi, J. I. Svendsen, A. Solheim, E. S. Andersen, J. Milliman, J. Mangerud, R. L. Hooke, Late Quaternary sediment yield from the high Arctic Svalbard area. *J. Geol.* **103**, 1–17 (1995).
77. G. J. Chakrapani, R. K. Saini, Temporal and spatial variations in water discharge and sediment load in the Alaknanda and Bhagirathi Rivers in Himalaya, India. *J. Asian Earth Sci.* **35**, 545–553 (2009).
78. S. K. Jain, P. Singh, A. K. Saraf, S. M. Seth, Estimation of sediment yield for a rain, snow and glacier fed river in the Western Himalayan region. *Water Resour. Manag.* **17**, 377–393 (2003).
79. X. Lu, D. L. Higgitt, Sediment yield variability in the Upper Yangtze, China. *Earth Surf. Process. Landf. J. Br. Geomorphol. Res. Group* **24**, 1077–1093 (1999).


**Acknowledgments:** We thank X. Lu, O. Slaymaker, V. Vanacker, M. Fort, N. Muhammad, F. Ali, and the IAG DENUCHANGE working group for earlier discussions and field assistance. **Funding:** This study was supported by the National Natural Science Foundation of China (grant nos. 52479055, 92047303, and 51925901) and by the Fundamental Research Funds for the Central Universities, Peking University. D.L. acknowledges the visiting scientist position supported by the Foundation Herbette. **Author contributions:** D.L. and T.Z. conceived the study. D.L. wrote the original draft. D.L. and T.Z. performed the analysis and designed the figures. All authors contributed to ideas and edits of subsequent revisions. **Competing interests:** The authors declare that they have no competing interests. **Data and materials availability:** All data needed to evaluate the conclusions in the paper are present in the paper and/or the Supplementary Materials. Runoff and sediment yield data are available in the supplementary tables, and the raw data are sourced from the existing literature, hydrological data yearbooks published by the Ministry of Water Resources, China; the Water and Power Development Authority, Pakistan (WAPDA); the Department of Hydrology and Meteorology, Nepal; and the Central Water Commission (CWC), India. Information on glacier cover is available from the Randolph Glacier Inventory v6.0 (www.glims.org/RGI/). Information on permafrost cover is available from the National Tibetan Plateau Data Center (https://data.tpdc.ac.cn/en/data/5093d9ff-a5fc-4f10-a53f-c01e7b781368/). NDVI data are available from the NASA Earth Observation Data sources (GIMMS NDVI: https://glam1.gsfc.nasa.gov/; and MODIS NDVI: https://ladsweb.modaps.eosdis.nasa.gov/). Air temperature and precipitation data from the ERA-5 reanalysis climate dataset are available from the Copernicus Climate Data Store (https://cds.climate.copernicus.eu/). Meteorological station–observed climate data are available from the China Meteorological Administration (http://data.cma.cn/en). SRTM DEM dataset are available at https://earthexplorer.usgs.gov. PGA data are available at http://gmo.gfz-potsdam.de/pub/introduction/introduction_frame.html. Lithology erodibility is available from the Glim dataset of global lithologic distributions (*77*, *78*).

Submitted 21 August 2024
Accepted 24 October 2024
Published 27 November 2024
10.1126/sciadv.ads6196